Pressure Measurements on Twin Vertical Tails in Buffeting Flow

William E. Triplett*
McDonnell Aircraft Company, St. Louis, Missouri

Buffeting pressures were measured on the vertical tail surfaces of a 13% F-15 model in a low-speed wind tunnel. Test variables included dynamic pressure, aircraft angle of attack, vertical tail incidence, and rudder deflection. Pressure transducers were flush mounted on rigid and flexible tails. Steady and unsteady pressures were obtained from the transducers at levels as low as 0.1% full scale. The steady pressures were integrated for aerodynamic coefficients and the unsteady pressures were reduced to spectral densities. The pressures are maximum at approximately 22 deg angle of attack and are significantly affected by tail flexibility.

Introduction

CONTEMPORARY twin-tail fighter aircraft may encounter high-frequency oscillations caused by buffeting flow emanating from the wing during very high angle-of-attack maneuvering. The buffeting flow occurs when the air flow on the upper wing surface becomes detached. Air flow in the detached region becomes turbulent which gives rise to fluctuating pressures on the wing, and induced oscillating pressures on surfaces which are in the flow path.

The induced buffeting pressures are broadband random fluctuations with predominant frequencies associated with the primary air flow properties of the aircraft (e.g., vortex flow from inlets, snags, and other sharp corners). The excitation forces will act on tail surfaces embedded in this buffeting flow and large oscillatory responses will result at the resonant frequencies of the tail. The tail structure and equipment must be designed to tolerate these oscillations as on the F-15 and F-18. An active suppression system could alternately reduce the resultant loads to a noncritical level. In the development of such an active suppression system the buffeting pressures on the tail surface must be known quantitatively.

The F-15 aircraft experienced large vibrations of the vertical tails while conducting air combat maneuvers at high angle of attack during early service usage. Flight tests were conducted to reproduce and investigate the vibrations. The tests consisted of windup turns at 20,000 ft for angles of attack up to 40 deg. The buffet excitation was determined to be essentially a function of the wing leading-edge separation and the geometry of the wing, fuselage, and vertical tails. The maximum tail vibration occurred at about 22 deg angle of attack and was predominantly in the first torsion mode at 33 Hz.

Subsequent wind tunnel tests were conducted in the MCAIR Low Speed Wind Tunnel (LSWT) with the 13%-scale F-15 aerodynamic model. For part of the tests the rigid left boom, vertical tail, and stabilator were replaced with the flexible boom and vertical tail from the 13%-scale F-15 flutter model and a rigid balsa stabilator with scaled mass properties. These early tests demonstrated vertical tail responses which compared closely with the flight test data.

Flowfield characteristics in the vicinity of the vertical tail were investigated in these early wind tunnel tests using mold line tufts, fog (a mixture of liquid nitrogen and steam), and hot film anemometer measurements. Combining the results of these techniques, the flowfield characteristics were obtained for a wing angle of attack of 22 deg, as shown in Fig. 1.

Fog was injected into the airstream at three butt line (BL) locations by a vertical rake. Fog introduced at BL 40 flowed inboard of the vertical tail toward the aircraft centerline. Fog introduced at BL 78, near the gun bump, also flowed well inboard of the tail. When introduced at BL 122, the fog flowed inboard and struck the vertical tail at the top. In addition, the fog streamlines, introduced in a vertical plane, rotated (top inboard) as they moved aft. Rotation ceased at about 90 deg as the flow approached the aft end of the aircraft. Additional information on the previous flight and wind tunnel testing is given in Ref. 1. The current tests, described in this paper, are presented in more detail in Ref. 2.

The current pressure measurement wind tunnel tests were conducted with the following objectives:

1) measure steady and unsteady pressures acting on vertical tails in buffeting flow,

2) investigate the effect of tail flexibility on the buffeting pressures, and

3) reduce the steady and unsteady pressure data to a form suitable for use in response suppression system analyses.

Model and Test Setup

The wind tunnel tests were conducted with the 13%-scale F-15 aerodynamic model in the LSWT, which is a continuous flow tunnel with a closed throat test section vented to the atmosphere. The cross section is 8×12 ft. Test variables included dynamic pressure, aircraft angle of attack, vertical tail incidence, and rudder deflection. Pressure transducers were flush mounted on rigid and flexible vertical tails. Strain gages were employed for bending, torsion, and shear loads.

The right-hand "pressure" tail and the left-hand "loads" tail are shown in detail in Fig. 2. The pressure tail is solid aluminum. It was numerically machined to provide channels for the pressure transducers and their leads. Thirty-nine transducers were mounted in five chordwise strips on each side of the tail in essentially the same locations. The transducer locations were based on an investigation to determine the accuracy of aerodynamic lift-curve slope with pressure tap distribution.

Double-face tape was used under the pressure transducers and the channels for the leads were filled with wax. A vibration test verified the suitability of this method of attachment and eliminated the concern over possible relative motion between the tail and the transducers. The leads entered the center section of the tail, which has removable covers, and emerged at the base of the tail on the inside. The leads were formed into a cable which interfaced with the tunnel data acquisition system.

Presented as Paper 82-0641 at the AIAA/ASME/ASCE 23rd Structures, Structural Dynamics and Materials Conference, New Orleans, La., May 10-12, 1982; submitted May 28, 1982; revision received May 5, 1983.

*Senior Staff Engineer, Structural Dynamics. Associate Fellow AIAA.

The left-hand loads tail, also made of solid aluminum, was instrumented with strain gages at the base of the tail at the elastic axis. Total tail aerodynamic coefficients were obtained from this loads tail to compare with integrated coefficients obtained from the pressure tail. Tufts were used on the loads tail for visibility of the buffeting flow patterns. Adjustable rudders were mounted on both tails and provisions were made for varying the vertical tail incidence. A hinge moment strain gage was provided for the loads tail rudder.

Specific transducer locations are shown in Fig. 3. The transducers on the inboard side are 0.25 in. lower than those on the outboard side. This offset was necessary because of insufficient tail thickness. The channels were routed, as illustrated in Fig. 2, so as to avoid soft spots beneath the transducers.

For some of the runs, the left-hand loads tail was replaced by a "flexible pressure" tail. The rigid left boom, vertical tail, and stabilator of the 13% F-15 aerodynamic model were replaced with the flexible boom and vertical tail from a 13% F-15 flutter model and a rigid stabilator with scaled mass properties. This is the same aeroelastic model that was used in the previous wind tunnel tests.

The flexible vertical tail structure, shown in Fig. 4, consists of a single magnesium spar, symmetrical about the elastic axis, and scaled to provide the proper stiffness distribution. The spar is attached through a fin root spring fitting to the flexible tail boom structure, which is then attached to the rigid aft fuselage bulkhead.

The tail is segmented into seven spanwise sections, arranged normal to the elastic axis. All seven sections are solid balsa wood. Provisions are present for attaching a rudder and a tip pod. The rudder has variable hinge line rotational restraint springs. The weight and center of gravity location of the tip pod are variable.

Twelve pressure transducers were flush mounted in the solid balsa sections, at identical locations to those used with the fourth strip (78% span) of transducers on the rigid pressure tail, for assessing the effect of flexible motion on the measured pressures. Figure 4 shows the pressure transducers on the outboard side of the flexible tail.

The pressure transducers were Kulite model LQ-125-10. They are high-response, disk-type transducers with a full-scale pressure of 10.0 psi. Their response was linear in the range 0.0 to 0.3 psi which was pertinent to the present tests.

Test Program

The pressure measurement model is shown in Fig. 5 at a high angle of attack in the LSWT. Wind tunnel runs were made with the model for: 1) two dynamic pressures, $Q=8$ and 12 psf; 2) three vertical tail incidences, $\beta=+2$, $+7$, and -8 deg; 3) three rudder deflections, $\delta=+5$, 0, and -5 deg; and 4) a range of angle of attack, $\alpha=0\rightarrow35$ deg.

The data processing system is shown conceptually in Fig. 6. Steady-state and dynamic data were obtained from the same transducer signals. Low-pass filters (2 Hz first-order break), built into the data acquisition system, were used in the steady-state channels. High-pass filters (1.3 Hz first-order break) were used in the dynamic channels.

Special care was required to get accurate steady-state data from the pressure transducers at the very low levels of pressure measured in the test which were on the order of 0.1% of full scale. Short blows at steady tunnel temperatures were used to reduce the steady-state drift. The transducers were balanced to zero and recorded with the wind off before and after each tunnel blow.

Dynamic data were recorded for each run by the multiplexer for exactly 1 min after reaching a stationary condition in the tunnel. The low-pass filtered steady-state signals were sampled and the instantaneous values were continuously displayed on a two-page CRT terminal. Digital displays were available for all of the variables to use in monitoring the tests. The steady data were also stored on an

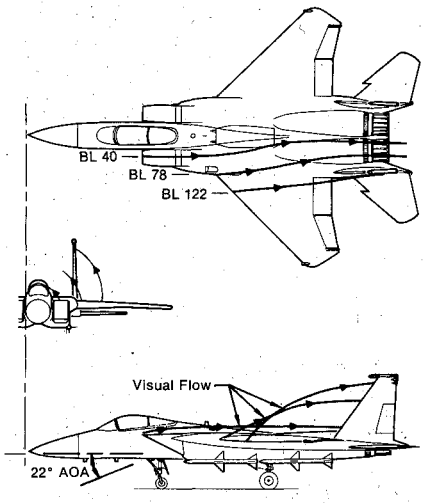

Fig. 1 Vertical tail flowfield characteristics, $\alpha=22$ deg.

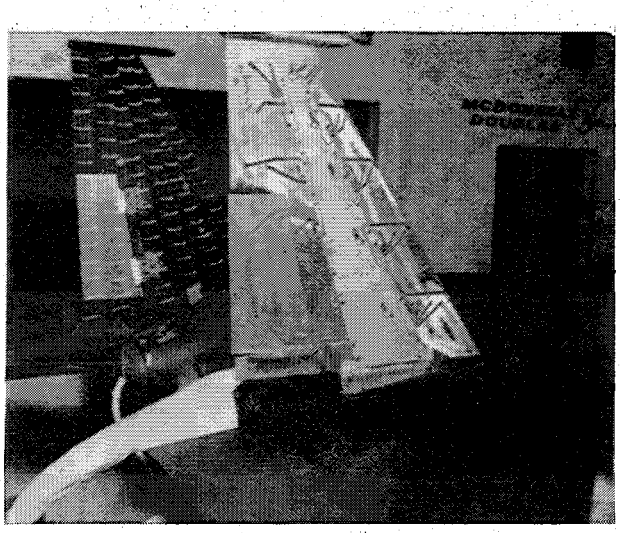

Fig. 2 Right-hand "pressure" tail and left-hand "loads" tail.

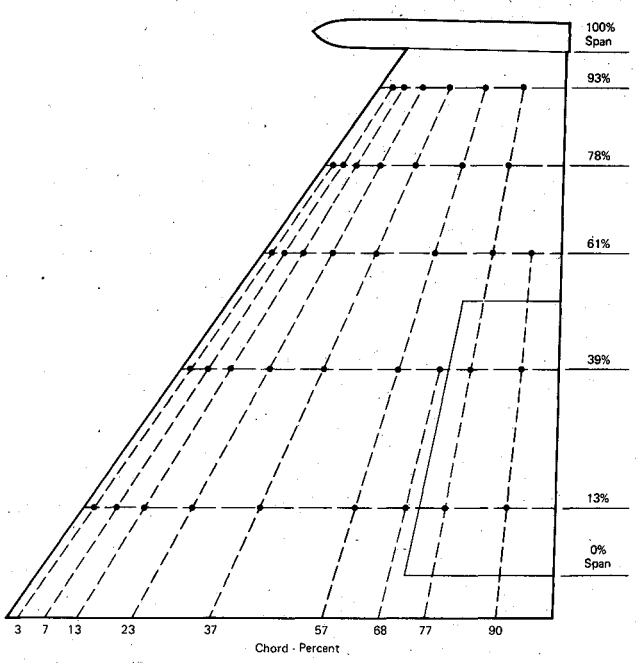

Fig. 3 Pressure transducer locations for rigid pressure tail.

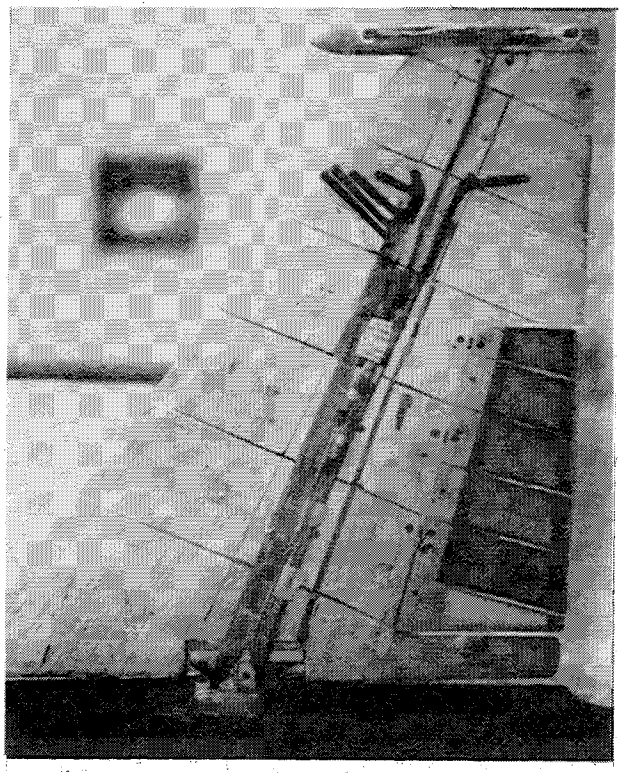

Fig. 4 Left-hand "flexible pressure" tail.

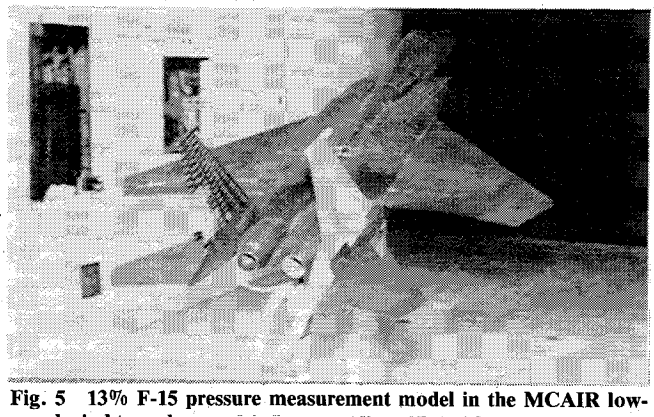

Fig. 5 13% F-15 pressure measurement model in the MCAIR low-speed wind tunnel.

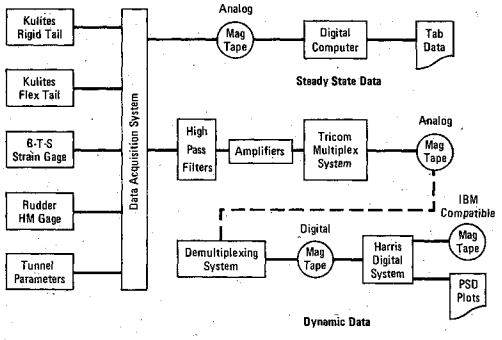

Fig. 6 Data processing system.

analog mag tape which was digitized and input to the on-site digital computer.

The on-site digital computer was programmed to give essentially on-line reduced steady-state pressure data, including plots of chordwise pressure distributions. The pressure distributions were integrated to give strip aerodynamic coefficients. Aerodynamic coefficients obtained from the loads tail strain gages were also available on-line.

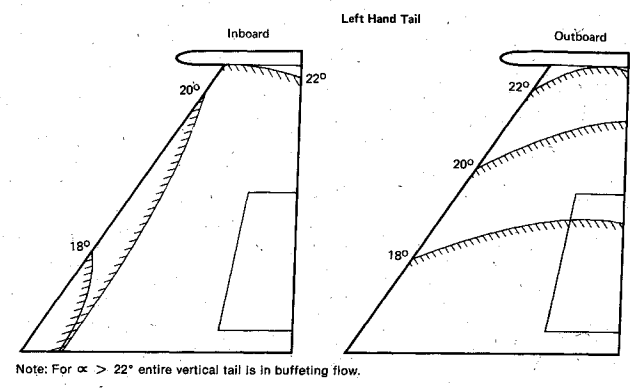

Fig. 7 Regions of buffeting flow based on tuft motion at various angles of attack.

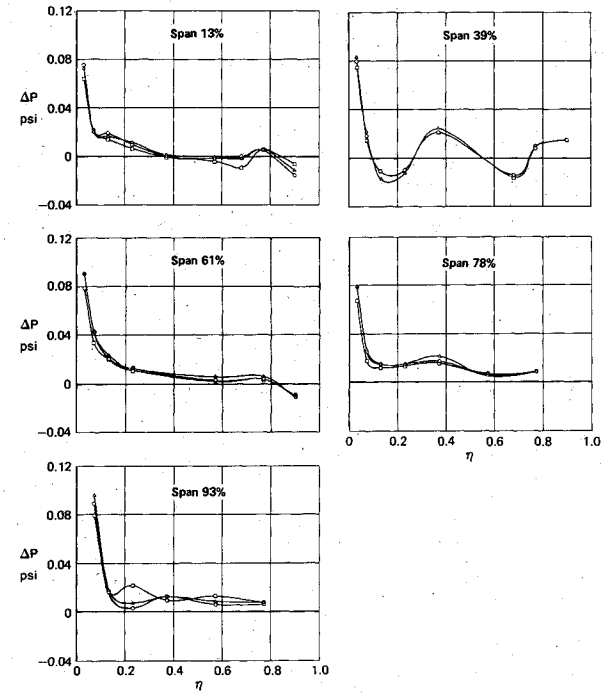

Fig. 8 Pressure distributions—check of repeatability; $Q = 12$ psf, $\beta = 2$ deg, $\delta = 0$ deg, and $\alpha = 0$ deg.

These data were invaluable during the test. An immediate evaluation of reduced test results was available while the model was still in the same test configuration.

The pressure tail was essentially problem free. The pressure transducers remained firmly in place during the entire test.

Steady-State Results

The tufts on the loads tail were used to provide information on the regions of buffeting flow. Observations of the flow patterns on both sides of the tufted tail for a range of angle of attack, combined with examination of photographs, determined the region of buffeting flow shown in Fig. 7. The buffet region begins at $\alpha = 18$ deg and completely covers the tail on both sides for $\alpha = 22$ deg and above.

The tunnel was remarkably noise free at the dynamic pressure of 12 psf which is only 10% of the operational capability. Tests at higher dynamic pressures were not advisable because of the danger of damage to the flexible tail and possible loss of pressure transducers on both rigid and flexible tails. It was demonstrated in the previous wind tunnel test that the flexible tail response is directly proportional to dynamic pressure so that higher levels were not necessary.

The Reynolds number at this dynamic pressure was 6.8×10^5/ft. Good comparisons between wind tunnel and

flight test responses[1] give assurance that the wind tunnel data is meaningful for the airplane at flight Reynolds numbers.

In this noise-free environment it was possible to get good repeatability of runs even at pressure levels near zero. Three widely separated runs with the same configuration at $\alpha = 0$ deg are shown in Fig. 8. ΔP is the inside minus outside pressure and is plotted vs nondimensional chord η for the five chordwise strips.

The steady-state pressure distributions for $\alpha = 0$ and 22 deg are shown in Fig. 9. This case was chosen for the baseline because maximum dynamic responses occur in both current and prior testing with the flexible tail at $\alpha = 22$-26 deg. Comparison shows higher levels of ΔP for the 22 deg case for the two lowest strips. The ΔP for the top three strips, however, are lower for the 22 deg case and the sign is reversed in the forward portion of the top two strips. The pressure changes are consistent with the flow patterns; inward at the top and outward at the bottom when the tail is immersed in the buffeting flow. Section lift coefficients, also shown in the figure, are calculated by the equation

$$C_L = \sum_{i=1}^{N} \frac{(\Delta P_i)(\Delta \eta_i)}{Q/144.0} \quad \text{positive outboard}$$

Good repeatability was also obtained when the tail was immersed in the buffeting flow. Figure 10 shows pressure distributions for two widely separated runs at $\alpha = 22$ deg and maximum dynamic pressure.

Steady pressure distributions are shown in Fig. 11 for the baseline case with both rigid and flexible pressure tails on the model. Pressure transducers were located at the same chordwise points for the 78% span strip on both tails. Comparison of the distributions at 78% span shows the significant effect of the tail flexibility on the impinging buffeting flow. The lift coefficient is three times larger for the flexible tail.

Sign conventions for the left-hand loads tail and the right-hand pressure tail are shown in Fig. 12. Resultant aerodynamic forces and moments acting on the left-hand loads tail, and rudder, are defined as:

F = side force (positive inboard), lb
M_B = root bending moment (positive along 47% chord elastic axis for tail tip inboard), ft lb
M_T = root torsion moment (positive about the elastic axis for leading edge inboard), ft lb
HM = rudder hinge moment (positive for trailing edge inboard), ft lb

Aerodynamic coefficients were calculated for the loads tail as follows:

C_F = side force coefficient = F/QS

C_{M_B} = root bending moment coefficient = $M_B/QS\ell_1$

C_{M_T} = root torsion coefficient = $M_T/QS\ell_2$

C_{HM} = rudder hinge moment coefficient = $HM/QS_r\ell_3$

where the tail area $S = 1.058$ ft^2, the tail span $\ell_1 = 1.341$ ft, the tail mean aerodynamic chord (MAC) $\ell_2 = 0.8775$ ft, the rudder area $S_r = 0.1685$ ft^2, the rudder MAC $\ell_3 = 0.3077$ ft, and the dynamic pressure $Q \sim$ psf.

Plots of the aerodynamic coefficients vs vertical tail incidence at $Q = 12$ psf and $\alpha = 22$ deg are shown in Fig. 13. Similar plots for rudder deflection are shown in Fig. 14. The curves are remarkably linear considering that the tail was completely immersed in buffeting flow. The resultant aerodynamic derivatives shown on the figures have reasonable values.

Aerodynamic force, moment about strip leading edge, and center of pressure for each strip of pressure transducers were

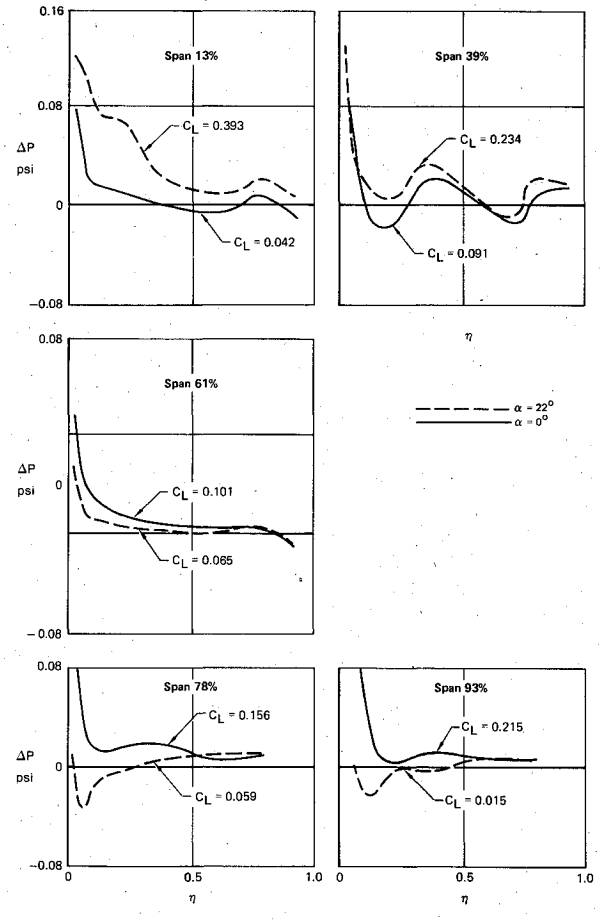

Fig. 9 Effect of aircraft angle of attack on pressure distributions; $Q = 12$ psf, $\beta = 2$ deg, and $\delta = 0$ deg.

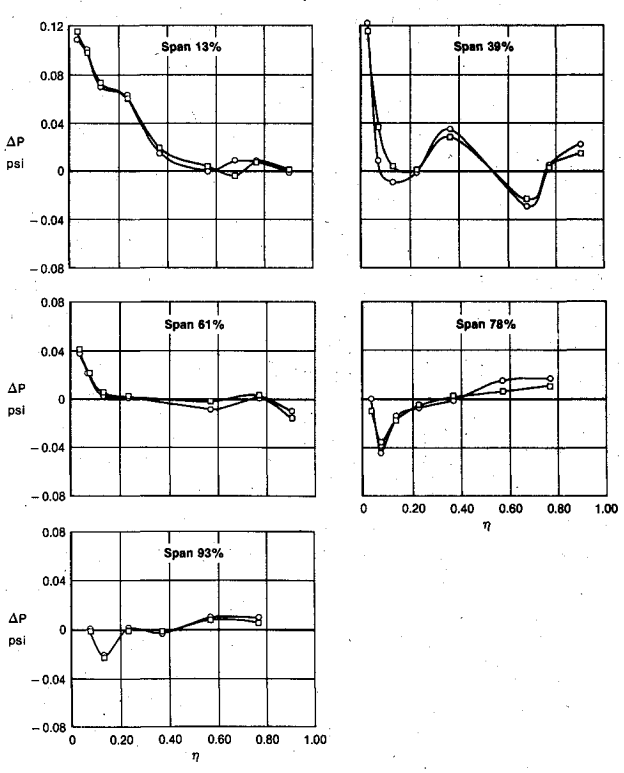

Fig. 10 Pressure distributions—check of repeatability; $Q = 12$ psf, $\beta = 2$ deg, $\delta = -5$ deg, $\alpha = 22$ deg.

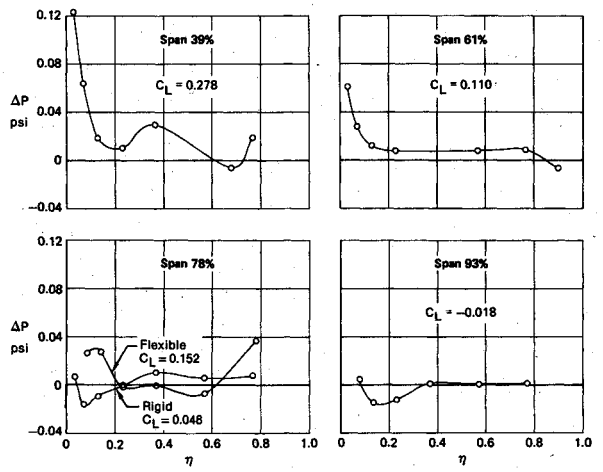

Fig. 11 Pressure distributions including flexible tail strip at 78% span; $Q = 12$ psf, $\beta = 2$ deg, $\delta = 0$ deg, and $\alpha = 22$ deg.

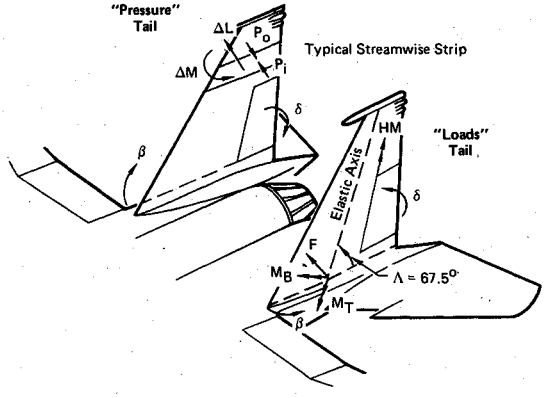

Fig. 12 Sign convention, right-hand pressure tail and left-hand loads tail.

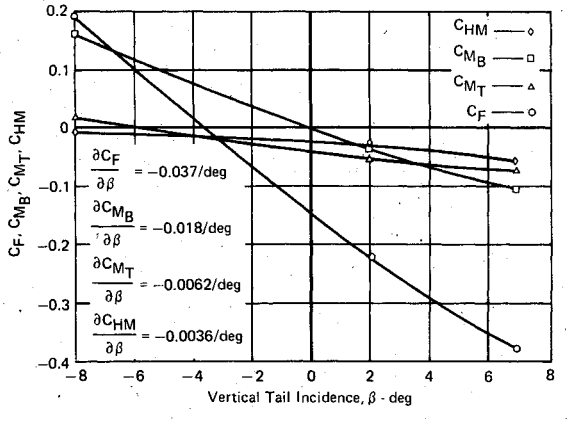

Fig. 13 Aerodynamic coefficients as functions of vertical tail incidence; $Q = 12$ psf, $\alpha = 22$ deg, and $\delta = 0$ deg.

calculated as follows:

$$C_L = \sum_{j=1}^{N} (P_{\text{inside}} - P_{\text{outside}})(\Delta\eta_j) \Big/ (Q/144)$$

positive outboard

$$C_M = \sum_{j=1}^{N} (P_{\text{inside}} - P_{\text{outside}})(\Delta\eta_j)(\eta_j) \Big/ (Q/144)$$

positive leading edge inboard

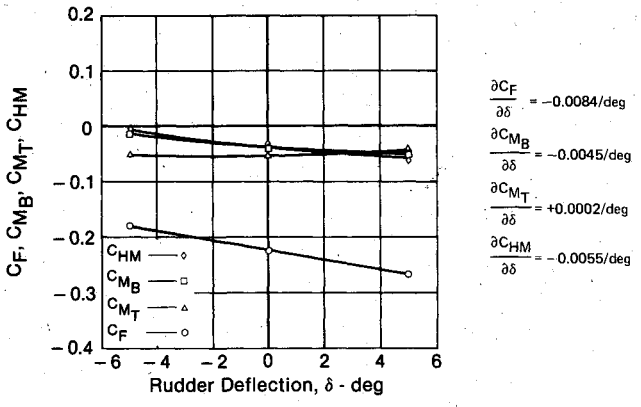

Fig. 14 Aerodynamic coefficients as functions of rudder deflection; $Q = 12$ psf, $\alpha = 22$ deg, and $\beta = 2$ deg.

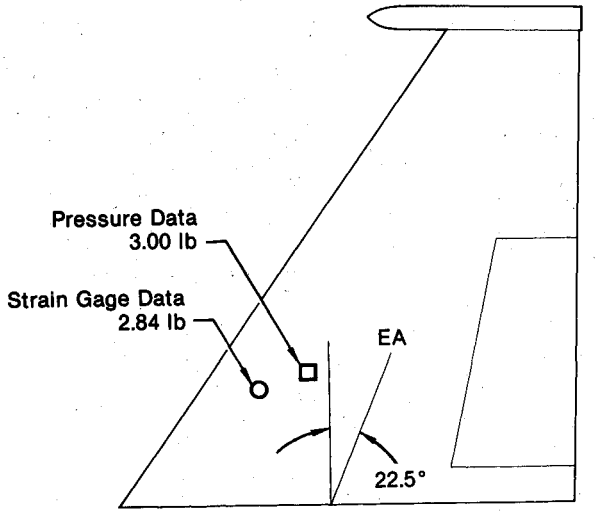

Fig. 15 Steady aerodynamic forces in buffeting flow; $Q = 12$ psf, $\beta = 2$ deg, $\delta = 0$ deg, and $\alpha = 22$ deg.

$\eta_{CP} = C_M / C_L$ positive aft of leading edge as fraction of strip chord

where η_j is the percent chord at the transducer location, and $\Delta\eta_j$ is the distance between midpoints along the chord, except at the leading and trailing edges where the distance was extended to the airfoil edge. Inoperative pressure transducers were accounted for by adding one half of the $\Delta\eta_j$ to the transducers on either side.

Forces and moments were calculated for the entire tail by summation of the individual integrated strip data. The force magnitude and location calculated from the pressure data is shown in Fig. 15 compared with similar data obtained from the strain gage measurements at the base of the left-hand loads tail. The forces agree within 6%. The center of pressure agrees within 4% of the span and 10% of the mean aerodynamic chord. A better comparison could be obtained by improved integration but the comparison is essentially limited by the sparseness of the pressure points.

Unsteady Results

Dynamic data were reduced to power spectral densities (PSDs) and cross spectral densities (CSDs) for the baseline case of $\alpha = 22$ deg and $Q = 12$ psf. The spectral densities were calculated with a frequency resolution of $\Delta f = 0.25$ Hz from 0 to 128 Hz. The total available record time of $T = 60$ s was used with a sample time of $\Delta t = 3900$ μs. This gives an 80% confidence factor for the ratio of measured to true value between

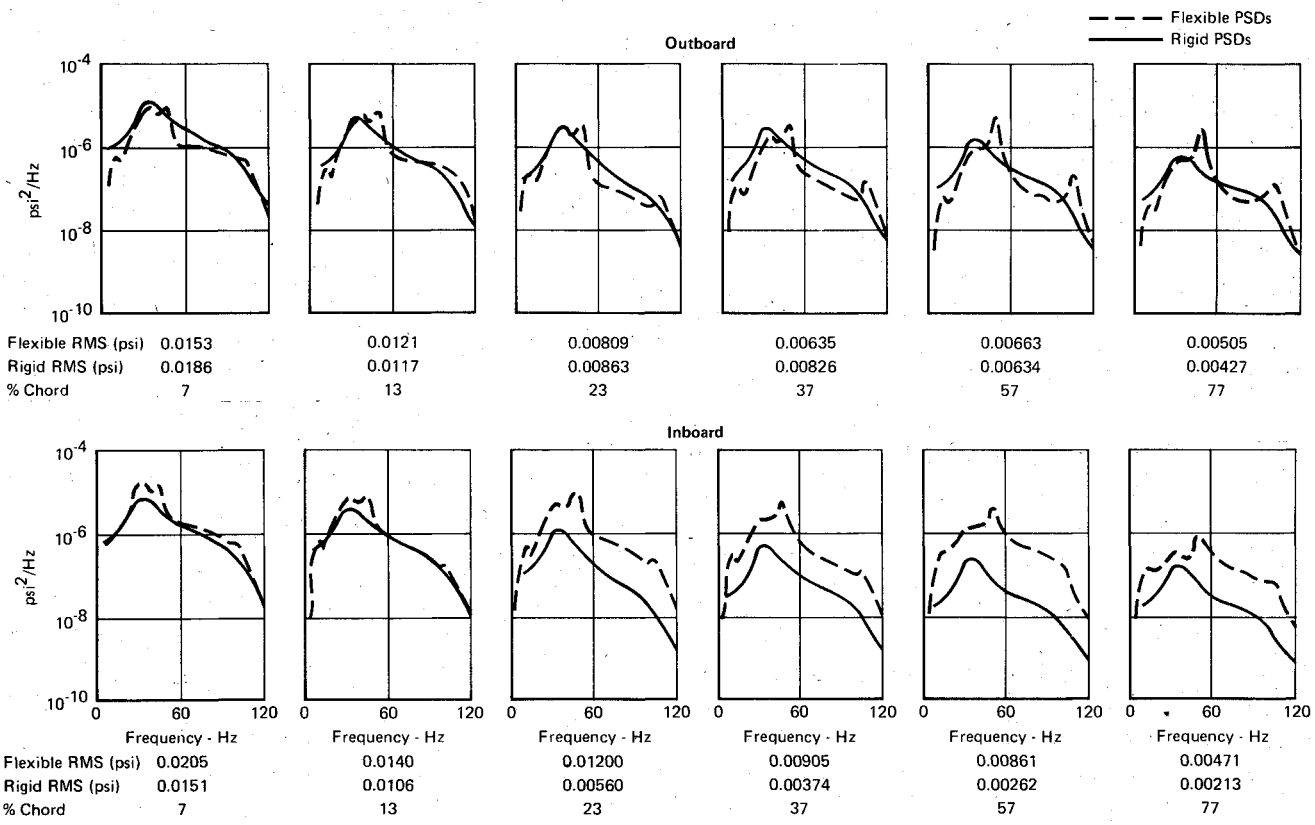

Fig. 16 Rigid and flexible tail PSDs for strip at 78% span; $Q = 12$ psf, $\beta = 2$ deg, $\delta = 0$ deg, and $\alpha = 22$ deg.

0.82 and 1.25 or alternately a 99% confidence factor for the ratio between 0.65 and 1.65 based on χ^2 distribution.

PSDs are shown for the strip of transducers at 78% span for both rigid and flexible tails in Fig. 16. The peak data for the rigid tail varies on the outboard side from 10^{-5} psi²/Hz at 7% chord to 10^{-6} psi²/Hz at 77% chord and on the inboard side from 10^{-5} to 10^{-7} psi²/Hz for the same stations. Root mean squares (RMS), obtained by integrating the PSDs, are shown below each graph.

The overall shape of the PSDs is similar for both rigid and flexible tails. There is a broad hump centered around 30 Hz which is characteristic of the impinging flow because it is present in both rigid and flexible data.

Distinct resonant peaks are present in the flexible tail PSDs. The flexible tail PSDs have resonances at 13 Hz (model first bending), 46 Hz (model first torsion), and a higher mode near 100 Hz. PSD levels for the flexible and rigid tails are similar on the outboard side while the PSDs are higher for the flexible tail on the inboard side, by as much as an order of magnitude at some stations toward the trailing edge.

Concluding Remarks

The principal conclusions supported by these wind tunnel tests are:

1) For the configuration tested, the pressures and associated vibration response levels reach a maximum at approximately 22 deg angle of attack and the predominant vibration mode is tail first torsion.

2) Measurement of both steady and unsteady pressures is feasible with the Kulite pressure transducers even if levels are on the order of 0.1% of full scale.

3) Tail flexibility has a significant effect on the impinging buffeting flow pressures; the steady pressures are modified in both magnitude and distribution and the PSDs are generally higher, by as much as an order of magnitude for some stations on the inboard side.

These wind tunnel tests were designed to furnish information on both steady and unsteady pressures acting on a surface located in a region of turbulent buffeting flow. The reduced data were intended to support the analysis and design of an active vertical tail torsional oscillation suppression system since there is no available aerodynamic theory to model this environment.

The measurements are valuable, however, for other reasons. They give insight into the environment for surfaces in a region of buffeting flow and are available for use in the design and development of future twin-tail aircraft.

Acknowledgment

This work was partially sponsored by the Air Force Wright Aeronautical Laboratories (AFWAL).

References

[1]Roos, H. N. and Waymon, G. R., "Testing for Severe Aerodynamically Induced Vibration Environments," Paper presented at 53rd Shock and Vibration Symposium, Danvers, Mass., Oct. 1982.

[2]Triplett, W. E., "Pressure Measurements on Twin Vertical Tails in Buffeting Flow; Vol. I—General Description, Vol. II—Test Data," AFWAL-TR-82-3015, April 1982.